Available online at www.sciencedirect.com
ScienceDirect
Lithos 91 (2006) 137–149
LITHOS
www.elsevier.com/locate/lithos

The transition from peraluminous to peralkaline granitic melts: Evidence from melt inclusions and accessory minerals

R. Thomas [a,*], J.D. Webster [b], D. Rhede [a], W. Seifert [a], K. Rickers [a,c], H.-J. Förster [d], W. Heinrich [a], P. Davidson [e]

[a] *GeoForschungsZentrum Potsdam, Telegrafenberg, D-14473 Potsdam, Germany*
[b] *American Museum of Natural History, Department of Earth and Planetary Sciences, Central Park West at 79th Street, New York, NY 10024-5192, USA*
[c] *Hamburger Synchrotronstrahlungslabor HASYLAB at Deutsches Elektronen-Synchrotron DESY, Notkestrasse 85, D-22603 Hamburg, Germany*
[d] *Institute of Earth Sciences, University of Potsdam, P.O. Box 601553, D-14415 Potsdam, Germany*
[e] *ARC Centre of Excellence in Ore Deposits, University of Tasmania, Hobart 7001, Australia*

Received 2 August 2005; accepted 13 March 2006
Available online 19 May 2006

Abstract

Fractional crystallization of peraluminous F- and H_2O-rich granite magmas progressively enriches the remaining melt with volatiles. We show that, at saturation, the melt may separate into two immiscible conjugate melt fractions, one of the fractions shows increasing peraluminosity and the other increasing peralkalinity. These melt fractions also fractionate the incompatible elements to significantly different degrees. Coexisting melt fractions have differing chemical and physical properties and, due to their high density and viscosity contrasts, they will tend to separate readily from each other. Once separated, each melt fraction evolves independently in response to changing T/P/X conditions and further immiscibility events may occur, each generating its own conjugate pair of melt fractions. The strongly peralkaline melt fractions in particular are very reactive and commonly react until equilibrium is attained. Consequently, the peralkaline melt fraction is commonly preserved only in the isolated melt and mineral inclusions.

We demonstrate that the differences between melt fractions that can be seen most clearly in differing melt inclusion compositions are also visible in the composition of the resulting ore-forming and accessory minerals, and are visible on scales from a few micrometers to hundreds of meters.

Keywords: Granite melts; Magma evolution; Melt inclusions; Melt–melt immiscibility; Peraluminosity; Peralkalinity; Accessory minerals

1. Introduction

In this paper, we demonstrate the formation of strongly peralkaline melt fractions by fractional crystallization and melt–melt immiscibility in peraluminous, water- and fluorine-rich albite granites and granite-related pegmatites. We also show that these processes may strongly influence the subsequent crystallization of granites, formation of pegmatites, and associated metasomatic and mineralization processes.

The B-, F- and P_2O_5-rich, Variscan, S-type Li-mica granites of Ehrenfriedersdorf and Eibenstock in the

* Corresponding author. Tel.: +49 331 288 1425; fax: +49 331 288 1474.
E-mail address: thomas@gfz-potsdam.de (R. Thomas).

0024-4937/$ - see front matter © 2006 Elsevier B.V. All rights reserved.
doi:10.1016/j.lithos.2006.03.013

central and western Erzgebirge of Germany have peraluminous bulk-rock compositions, indicated by an aluminium saturation index [ASI, moles $Al_2O_3/(CaO+Na_2O+K_2O+Rb_2O+Cs_2O)$] between 1.17 and 1.36. Evolved Li-mica granites in the eastern Erzgebirge, which are later in the regional magmatic cycle and associated with zones of crustal extension, are less peraluminous. These high-F, low-P_2O_5 Li-mica granites of A-type affinity are characterized by up to 0.9 wt.% F in the bulk rock and ASI values between 1.00 and 1.15.

Melt inclusions (MIs) are small droplets of silicate melt trapped within phenocrysts at magmatic temperatures and pressures (Lowenstern, 2003). Relatively stable phenocryst hosts such as quartz act as "pressure vessels", helping to preserve the original magmatic volatile abundances. In recent years, improvements in various analytical techniques made it possible to study small MIs (≤ 10 μm). One important advantage is the determination of water concentrations in small MIs deep in the host using confocal micro-Raman spectroscopy, which can be used for concentrations from 0.01 to >25 wt.% (Thomas, 2000; Thomas et al., 2006b). Recent studies (e.g., Thomas et al., 2000, 2003, 2005, Rickers et al., 2006) have found significant differences in composition between the bulk-rock composition and MIs within the same rocks. Furthermore, even in syngenetic MIs within single growth zones in quartz crystals, large differences in the concentration of volatiles such as H_2O, F, B, Cl and the alkalis have been observed.

During MI studies of Variscan granites and pegmatites, we have commonly observed two contrasting melt inclusion types in quartz, characterized by different filling degrees (see Fig. 1) and chemical composition (as indicated by different mineral phases). After re-homogenization, we often observed both MIs with peraluminous composition (consistent with the bulk-rock composition) and MIs with an ASI<1.0, or with a molar peralkaline index $[(Na_2O+K_2O)/Al_2O_3]$ >1. The occurrence of two distinct populations of MIs indicates that the bulk composition of the rocks, and the composition of the magmatic liquids trapped as MIs, was significantly different. These results are supported by apparently unusual mineralogical observations, i.e., the occurrence of nepheline and leucite in quartz, the extreme enrichment of some trace and ore-forming elements, and the generation of water-rich melts with very low densities and viscosities (Thomas et al., 2000, 2003, 2005; Webster et al., 2004). Thus, studies of MIs shed light onto important facets of magmatic evolution usually invisible in studies based entirely on bulk-rock samples.

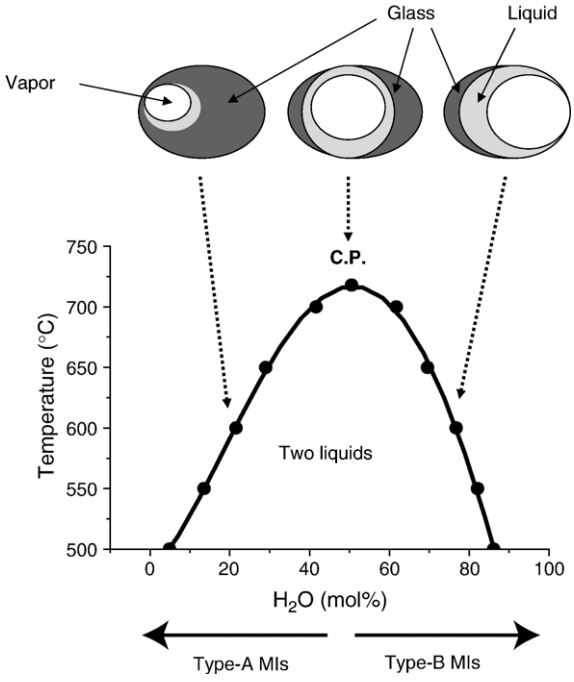

Fig. 1. Schematic characteristics of three different types of melt inclusions (type-A, near critical, and type-B) at room temperature (after re-homogenization). The dotted arrows show schematic degrees of filling in relationship to the pseudobinary melt–H_2O system. Solid arrows show the relation to the respective inclusion types.

In this paper, the origin of cogenetic, peraluminous and peralkaline melt fractions and their general significance is demonstrated, using primarily samples from two localities in the German Erzgebirge, peralkaline and peraluminous pegmatites from Ehrenfriedersdorf and topaz–zinnwaldite–albite granites from Zinnwald. To demonstrate that the observations have general validity and are not restricted to a few exotic occurrences, results from other occurrences/deposits are additionally presented.

2. Ehrenfriedersdorf pegmatites

2.1. Immiscibility processes

MI studies (Thomas et al., 2000, 2003) have shown that progressive differentiation and volatile enrichment drove the Ehrenfriedersdorf granite–pegmatite system to a solvus, where two "first-order" pegmatite-forming melts coexisted. The critical point of this solvus is at about 712 °C, 100 MPa, 20 wt.% H_2O, and 4.1 wt.% B_2O_3. Cooling and concomitant fractional crystallization from 700 to 500 °C induced development of two immiscible conjugate melts with contrasting properties: an H_2O-poor (type-A) and an H_2O-rich (type-B) melt

along the opening solvus (see Thomas et al., 2003, their Fig. 4). While cooling to about 500 °C from the critical point, relatively H_2O-poor melts with 20 to 2.4 wt.% H_2O coexist with H_2O-rich melts containing 20 to 44 wt.% H_2O (Thomas et al., 2000, 2003). The bulk chemical character of the coexisting melts changes simultaneously. With cooling and fractionation, the ASI of the type-A melts increases from metaluminous to strongly peraluminous values. For the type-B melts, this value evolves with cooling towards strong peralkaline characteristics (ASI_A/ASI_B increases from 1 at the critical point to ≈ 3 at 500 °C). In the following discussion, we use the terms peralkaline and peraluminous sensu stricto, strictly based on the ASI. We note, however, that in some cases we will discuss melts with more than 40 wt.% H_2O, in which H_2O may be more abundant than SiO_2. We consider these terms appropriate, because the extreme melts evolve towards more conventional compositions during fractional crystallization.

The type-B melts have low densities and viscosities relative to type-A melts, and will easily separate from them driven either by gravity or by compaction. They may pond near the roof of the magma body, or may migrate out along grain boundaries or open fissures. It is important to note that melt–melt immiscibility needs not happen only once during magmatic evolution.

An excellent example of multiple phase separation was given by Vogel (1977). Up to eight different microphases were detected in the $BaO–B_2O_3–SiO_2$ system. After primary separation, two phases of different viscosity are formed (droplets embedded in a glass matrix), which during cooling behave almost as two separate systems, with further separation processes of their own. The high viscosity of the matrix prevents the complete separation of the different phases.

The separation of a homogeneous phase into two or more immiscible phases presents interesting kinetic problems. Certain processes of diffusion and site-changing must occur, which enable "agglomeration" of particles to produce new conditions of concentration. When a liquid unmixes, the newly formed phases appear at first as a mere turbidity (Niggli, 1937). Subsequently, this unites to form an emulsion of droplets. If the phases possess different specific gravities, the heavier liquid will soon settle and separation into layers will result. Autonomous melt development occurs, if such a separate layer is tapped and moved away.

The observation in the Ehrenfriedersdorf pegmatites of coexisting MIs with contrasting compositions, but nearly the same water contents (Fig. 2), however at significantly lower *T* of about 600 °C, attests to near-critical conditions and formation of a second melt fraction in nature. The degree of separation of the two melts, required before the second solvus could be encountered, depends only on insufficient re-equilibration of the two melts. In nature, this is assured if the type-A and type-B melts separate by ponding within the pegmatite, or by the extrusion of type-B melts as discrete new pegmatite bodies. However, provided that diffusive transfer across the immiscible phase boundary is not excessive, each phase (since they have significantly different compositions) will evolve independently in response to changing pressure and temperature conditions. Thus, multiple and even serial immiscibility events are possible.

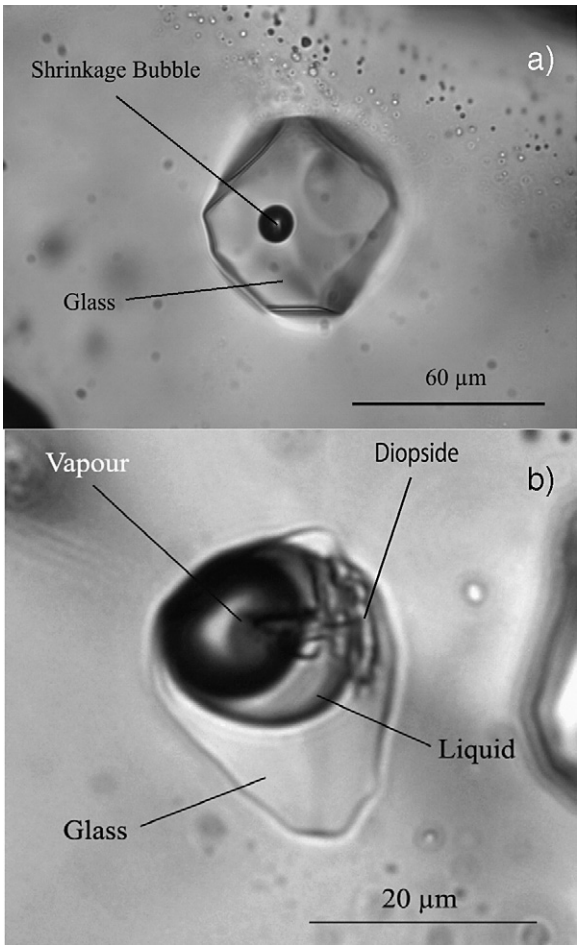

Fig. 2. Photomicrographs of type-A (a) and type-B (b) melt inclusions in pegmatite quartz (in the vicinity of the nepheline inclusions shown in Fig. 3) from Ehrenfriedersdorf, re-homogenized at 600 °C and 1 kbar. The glass of type-A melt inclusion contains 27.7±1.0 wt.% H_2O_T (total water), the glass of type-B MI contains 30.8±5 wt.% H_2O_T, demonstrating that both inclusions were trapped near the critical point of a second binary. The H_2O concentration was determined using Raman spectroscopy (see Thomas et al., 2006b).

2.2. Melt compositions

The conjugate type-A and -B melts are characterized by very strong chemical contrasts (see Table 1). The detection of topaz in type-A MIs shows that Al and F are enriched in this melt, and the melt is slightly peraluminous. In contrast, diopside was identified by Raman spectroscopy in the coexisting type-B MIs demonstrating that this melt was Al-poor, but enriched in Ca, Mg, and alkalis, and therefore alkaline to peralkaline. Furthermore, type-B inclusions contain wolframoixiolite [(Fe,Mn,Nb)(Nb,W,Ta)O_4] and cassiterite as confirmed by Raman spectroscopy. Each of these two minerals occupies a volume of about 1% of the MI, showing a significant enrichment in Nb, W, Ta, and Sn, and the potential for the formation of economic ore deposits. In the Ehrenfriedersdorf (Sauberg) mine, steeply dipping, ≤10-cm-thick, zircon-rich beryl-quartz veins in the country rock only contain type-B MIs in quartz and beryl, demonstrating that such mobile metal-rich melt fractions can migrate after separation from the pegmatite or granite, and may form separate geological entities.

Table 1
Representative compositions of the bulk rock of the parental Greifenstein granite (Webster et al., 1997) and the melt inclusions in quartz from the Ehrenfriedersdorf pegmatite

	Granite bulk rock	Type-A melt inclusions in pegmatite quartz		Type-B melt inclusions in pegmatite quartz trapped near the critical point
Temp. (°C)	–	650	700	700
SiO_2	74.2	62.0±1.1	56.9±0.5	24.3±3.6 [a]
TiO_2	0.04	0.02	0.02	0.02 [a]
SnO_2	0.004	0.09±0.02	0.08	0.15
Al_2O_3	14.7	11.7±0.5	11.4±0.3	11.1±1.7 [a]
B_2O_3	0.004	3.4±0.5	3.7±0.6	4.1±0.2
FeO	1.0	0.29±0.05	0.24±0.02	3.7±0.4 [b]
MnO	0.02	0.04±0.01	0.04±0.01	0.5 [b]
BeO [c]	0.002	0.13	0.3	0.35 [a]
MgO	0.1	d.l.	d.l.	d.l.
CaO	0.5	0.03±0.01	0.03	0.8 [b]
Li_2O [c]	0.14	0.09	0.57	0.4 [b]
Na_2O	3.8	3.20±0.14	2.04±0.84	5.9±0.9
K_2O	4.2	3.00±0.55	4.33±1.32	7.5+1.1
Rb_2O	0.1	0.61±0.10	1.10±0.32	0.23 [b]
Cs_2O	n.d.	0.12±0.04	1.59±0.22	0.12 [b]
F	0.8	4.49±0.25	2.45±0.85	5.8±0.6 [a]
Cl	n.d.	0.14±0.02	0.10±0.03	6.7±1.0
P_2O_5	0.54	3.20±0.31	1.14±0.13	6.7±0.7 [a]
H_2O	(<1.0)	9.8±1.2	16.2±0.9	24.0±2.5
Sum	100.15	102.53	102.23	102.37
Sum [d]	99.81	100.61	100.98	98.42
ASI [e]	1.23	1.26±0.11	1.02±0.27	0.53±0.10
n	4	10	5	10

Homogenization temperatures and water concentrations of type-A and-B melts are from Thomas et al. (2000).
d.l.: detection limit; n.d.: not detected; *n*: number of measured melt inclusions; standard deviations were calculated from repeated measurements.
[a] Values of the glassy part assuming that concentrations in the liquid part are small.
[b] Minimum values because concentration in the liquid part could not be determined.
[c] Determined by SIMS at Woods Hole Oceanographic Institution, MA, USA by J. Webster (see also Webster et al., 1997).
[d] Sum corrected for F and Cl.
[e] ASI—aluminum saturation index {moles of [Al_2O_3/($CaO+Li_2O+Na_2O+K_2O+Rb_2O+Cs_2O$)]}.

In some areas inside or outside those pegmatite bodies unaffected by alteration (greisenization) processes, miarolitic cavities (up to several tens of centimeters) contain prismatic cassiterite (up to 5 cm in length), huebnerite, wolframoixiolite, Nb-tantalite, zircon, monazite, xenotime, REE-rich fluorite and other phases. Borax [$Na_2B_4O_5(OH)_4*8H_2O$] is occasionally observed between the cassiterite crystals indicating that the greisenization process was minimal, the mineral-forming melt was rich in volatiles (particularly in type-B melts) and had a peralkaline character (see also Schmidt et al., 2005). This high-temperature ore mineralization in such miarolitic cavities is related to the type-B melt evolution, as indicated by the dominance of type-B MIs with trapping temperatures between 650 and 600 °C. Age determinations on monazite and xenotime show that the miarolitic cavities have the same age as the main pegmatite, for which a U–Th–total Pb chemical age and an U/Pb isotopic age of 320±2 Ma (2σ) was obtained (Romer and Thomas, 2005a,b). Th-poor uraninite (ThO_2 ~4 wt%), exclusively found in peraluminous environments, yields a chemical age of 320±4 Ma. For the pegmatite-hosting granite, Romer and Thomas (2005b) have determined a $^{206}Pb/^{238}U$ monazite age of 323.9±3.5 Ma (2σ), demonstrating that the pegmatites are directly related to the main granites.

2.3. Compositions of accessory minerals from contrasting melt fractions

Melt-inclusion studies have shown that the equilibrium crystallization of a volatile-rich pegmatitic melt can force the primary homogeneous melt to split into two immiscible melt fractions with strongly different physical and chemical properties. To investigate whether these differences are reflected in the composition of associated accessory minerals, we have analyzed two examples, characterized by the dominance of each of the two endmember cases: bulk peraluminosity (feldspar,

quartz, topaz, mica) and bulk peralkalinity (coexistence of quartz and K-feldspar with nepheline and diopside).

2.3.1. The peraluminous trend

The mineralogical consequences of peraluminous melt evolution include melt pockets separated by large K-feldspar crystals. These, centimetres to decimetre pockets are peraluminous in composition, and occur as fine-grained, unidirectional solidification textures composed mainly of feldspar, quartz, and mica. We interpret these pockets as crystallized type-A melt. In pockets unaltered by pervasive post-pegmatite hydrothermal fluids, accessory minerals (uraninite, monazite, xenotime, zircon, cassiterite) of the peraluminous melt evolution have survived. The main characteristics of some of the accessory minerals are given in Tables 2a and 2b.

Table 2a
Composition (wt.%) of zircon crystallized from peraluminous type-A melt and peralkaline type-B melt fractions from the Ehrenfriedersdorf pegmatite and the Zinnwald topaz–albite granite

	d.l.	Ehrenfriedersdorf pegmatite		Zinnwald topaz–albite granite	
		Type-A melt	Type-B melt	Type-A melt	Type-B melt
WO_3	0.16	d.l.	1.92	0.41	2.45
P_2O_5	0.09	d.l.	1.49	0.10	3.00
Nb_2O_5	0.09	d.l.	1.25	d.l.	0.94
Ta_2O_5	0.15	d.l.	0.19	0.10	0.49
SiO_2	0.04	30.42	19.76	28.40	19.74
ZrO_2	0.11	61.64	35.97	55.68	35.01
HfO_2	0.14	2.45	15.13	4.97	6.38
ThO_2	0.08	0.43	0.47	0.40	5.53
UO_2	0.10	0.99	2.51	2.19	0.88
Al_2O_3	0.02	0.21	0.83	0.75	1.45
Fe_2O_3	0.06	0.41	0.80	0.49	1.36
Sc_2O_3	0.03	0.13	0.49	0.12	0.75
Y_2O_3	0.05	0.41	2.31	0.03	3.40
Ce_2O_3	0.08	0.03	0.18	0.03	1.39
Nd_2O_3	0.10	0.03	0.06	0.02	0.11
Sm_2O_3	0.12	0.08	0.13	d.l.	0.08
Gd_2O_3	0.12	0.07	0.51	0.05	0.61
Tb_2O_3	0.12	d.l.	0.44	0.07	0.12
Dy_2O_3	0.13	0.14	0.90	0.01	0.83
Ho_2O_3	0.14	d.l.	0.12	d.l.	0.18
Yb_2O_3	0.08	0.08	1.80	0.61	2.99
Lu_2O_3	0.08	0.00	0.22	0.11	0.44
CaO	0.03	0.27	3.12	0.99	0.57
MnO	0.06	d.l.	d.l.	0.43	0.10
PbO	0.06	d.l.	0.03	0.17	0.06
F	0.07	d.l.	d.l.	0.27	1.87
Total		97.79	90.63	96.36	89.99
$\Sigma REE_2O_3+Y_2O_3$		0.84	6.67	0.93	10.15
Zr/Hf		22.0	2.1	9.8	4.8
Th/U		0.4	0.2	0.2	6.3

d.l.—detection limit (20 kV, 40 nA).

2.3.2. The peralkaline trend

The occurrence of 0.5-mm-long nepheline aggregates in quartz and feldspar (Thomas et al., 2003) is an important indication for the presence of peralkaline melt fractions. The nepheline shows aegirine+kalsilite exsolution textures and a thin reaction rim of K-feldspar, where it is in contact with surrounding quartz (Fig. 3). The composition of nepheline, along with the composition of the K-feldspar rim between nepheline and pegmatite quartz, is given in Table 3.

Although the Sauberg pegmatite has a dominantly peraluminous character, it contains areas with strongly peralkaline composition, as indicated by type-B MI in quartz, as well as by carbonate/bicarbonate-rich MI in cassiterite, with homogenization temperatures of about 600–650 °C. The survival of this primary paragenesis is relatively rare in the Sn–W deposit of Ehrenfriedersdorf, because of overprinting by late pneumatolytic alteration and mineralization fluids at about 400 °C across the whole deposit (Thomas and Tischendorf, 1987). One of the samples from the Sauberg mine is composed of quartz, traces of orthoclase, large cassiterite crystals (up to 5 cm long), wolframite, Nb-tantalates, bismuth, bismuthine, hematite, REE-rich fluorite, topaz, albite, zircon, monazite, and xenotime. It clearly shows a pegmatitic texture and comes from a miarolitic cavity in the studied pegmatite. It is different in appearance to that of peraluminous pegmatites in the Ehrenfriedersdorf deposit (see Oelsner, 1952). Nb-rich cassiterite started to crystallize together with wolframoixiolite and Nb-tantalates. A second generation of cassiterite formed in association with wolframite.

The paragenesis, composition and habit of the main ore minerals from the miaroles of the Ehrenfriedersdorf granite show many peculiarities in comparison with the features of the typical ore minerals of the Ehrenfriedersdorf Sn–W deposit. Cassiterite grains from this deposit are usually small, prismatic (up to 5 mm) and frequently form twins, the so-called “Visiergraupen” (beak of tin). The trace element concentration of this cassiterite is very low. In contrast, the cassiterite from the peralkaline zones forms up to 5 cm long prismatic crystals and contains high amounts of Nb (0.81 wt.% Nb_2O_5) and Ta (0.26 wt.% Ta_2O_5). Also the composition of wolframite differs strongly between the main ore body and the peralkaline pegmatites: while the hübnerite/ferberite molar ratio, i.e., the ratio Mn/(Mn+Fe), is 0.60 in the pegmatites, it is as low as 0.20 in the main peraluminous mineralization (see Oelsner, 1952).

Another unusual mineral, which occurs as relics in the centre of large apatite aggregates in the Ehrenfriedersdorf (Sauberg) pegmatite, is Sr-rich apatite containing up to 35.4 wt.% SrO. Such Sr-rich apatites

Table 2b
Average composition (in wt.%) of monazite and xenotime from the Ehrenfriedersdorf pegmatite (ED) and xenotime from the Zinnwald granite (ZW)

Melt type	d.l.	Peraluminous	Peralkaline	Peraluminous	Peralkaline	Peraluminous	Peralkaline
		ED: monazite		ED: xenotime		ZW: xenotime	
P_2O_5	0.08	29.75	29.66	32.48	30.24	33.40	25.74
SiO_2	0.04	0.53	0.46	1.05	0.12	0.91	1.50
ThO_2	0.06	21.91	15.65	1.12	0.04	2.22	4.65
UO_2	0.05	3.69	0.53	3.35	0.41	0.81	0.39
Al_2O_3	0.03	0.02	0.01	0.00	0.00	0.01	0.00
Y_2O_3	0.05	2.74	0.70	41.60	22.97	42.74	27.06
La_2O_3	0.10	4.62	6.97	0.01	0.01	0.03	0.13
Ce_2O_3	0.10	15.39	20.84	0.05	0.01	0.10	0.53
Pr_2O_3	0.15	1.98	2.74	0.03	0.01	0.04	0.05
Nd_2O_3	0.14	7.03	9.78	0.33	0.09	0.35	0.35
Sm_2O_3	0.13	2.93	5.56	0.54	0.13	0.43	0.48
Gd_2O_3	0.13	2.20	2.53	4.28	5.75	3.79	3.55
Tb_2O_3	0.14	0.31	0.29	1.08	1.25	0.79	0.71
Dy_2O_3	0.14	0.89	0.56	6.99	9.90	5.37	6.60
Ho_2O_3	0.15	0.06	0.03	0.94	1.77	1.03	1.43
Er_2O_3	0.16	0.17	0.14	2.18	7.52	3.17	5.90
Yb_2O_3	0.11	0.02	0.03	1.65	14.21	2.13	8.26
Lu_2O_3	0.13	0.01	0.00	0.31	1.94	0.29	1.19
CaO	0.02	5.31	3.32	0.99	0.23	0.04	0.91
PbO	0.06	0.43	0.10	0.13	0.01	0.20	0.00
Total		99.99	99.90	99.11	96.61	97.85	89.43
LREE/HREE		8.7	12.8	0.06	0.01	0.06	0.06
Th/U		6.1	30.2	0.34	0.10	2.8	12.2
n		17	11	4	8	81	1

d.l.—detection limit (20 kV, 40 nA).

are more typical for nepheline syenites, alkaline to peralkaline pegmatites, and carbonatites (e.g., Dudkin et al., 1964; Bühn et al., 2001; Chakhmouradian and Mitchell, 2002). The mineral paragenesis in these peralkaline zones is consistent with the existence of discrete segregations of type-B melt on decimeter scales in the Ehrenfriedersdorf pegmatites.

2.3.3. Accessory minerals

Where relicts of both types of evolution are well-preserved, accessory minerals such as zircon, monazite, and xenotime exhibit distinctive compositions. All three minerals formed either from peraluminous or peralkaline melt fractions.

Zircon: The composition of zircon is remarkably variable (Table 2a). Zircon poor in Hf ($HfO_2 \leq 2.5$ wt.%) formed in peraluminous environments, while zircon from peralkaline melt fractions is enriched in Hf ($HfO_2 \sim 15$ wt.%). Elements such as U, Sc, Y, and Yb display a strong enrichment in "peralkaline" zircon.

Monazite: The composition of monazite from peraluminous environments is characterized by higher Th und U concentrations: 22 wt.% ThO_2 versus 16 wt.% in peralkaline melt fractions and 3.7 wt.% UO_2 versus 0.5 wt.% (Table 2b).

Xenotime: Grains from peraluminous environments are characterized by higher Th, U, and Y concentrations (1.1, 3.4 and 41.6 oxide wt.%, respectively) (see Table 2b). On the other hand, the heavy rare-earth elements (HREE) are strongly enriched in "peralkaline" xenotime.

Furthermore, "peralkaline" monazite and xenotime have experienced a loss of Pb, probably owing to the interaction with post-pegmatitic, $F–CO_2–NaHCO_3$-rich hydrothermal solutions of Cretaceous age (Romer and Thomas, in preparation).

The observed features of the main and accessory minerals are, in general, consistent with the characteristics of rare metal Nb–Ta–Zr–Hf–REE–U–Th deposits associated with peralkaline silicic rocks. The high level of F is responsible for depolymerization of the silicate melt and the complexation of the REEs and other high field strength (HFS) elements (Keppler, 1993; Mysen et al., 2004).

3. Topaz–zinnwaldite–albite granites at Zinnwald

3.1. Immiscibility processes

Previous studies of these highly evolved rocks demonstrated that the H_2O and F concentrations in

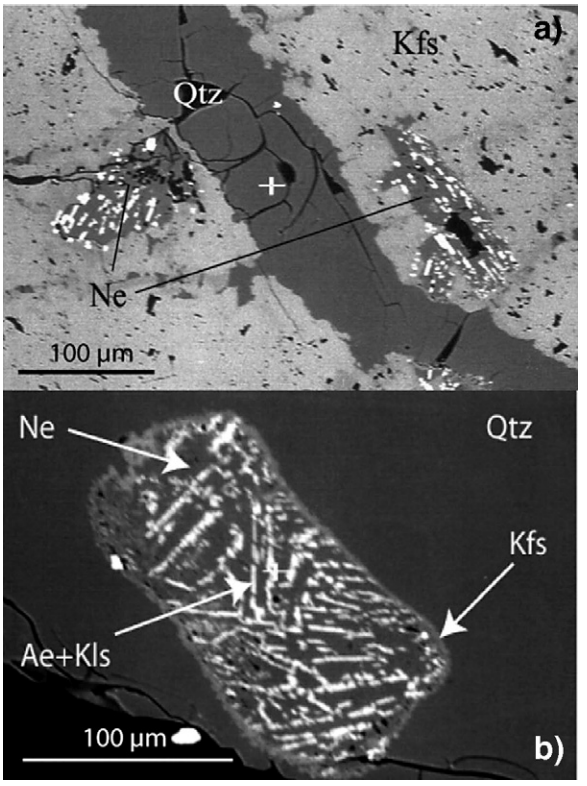

Fig. 3. Back-scattered electron images of nepheline inclusions in feldspar (a) and quartz (b) from the Ehrenfriedersdorf pegmatite. Nepheline shows kalsilite and aegirine exsolution lamellae.

their MIs increase with progressive crystallization (Webster et al., 2004; Thomas et al., 2005). If we construct an ASI versus F diagram from the MI data, three different trends are obtained (Fig. 4): Trend I displays a negative correlation between ASI and F up to a concentration of about 2.6 wt.% F (at 23 wt.% H_2O

Table 3
Compositions (in wt.%) of nepheline from a nepheline–kalsilite–aegirine exsolution and the kalifeldspar rim between nepheline and quartz from Ehrenfriedersdorf pegmatite (from Thomas et al., 2003)

	Nepheline (n=11)	K-feldspar rim
SiO_2	45.8±1.4	68.5
Al_2O_3	31.8±0.4	16.6
FeO	0.3±0.1	0.4
Na_2O	17.1±0.1	3.2
K_2O	3.8±0.3	9.1
Rb_2O	0.2±0.04	0.2
P_2O_5	~ 0.02	0.02
Total	99.02	98.02
X_{Ne}	0.86	
X_{Ks}	0.14	
X_{Or}		0.65
X_{Ab}		0.35

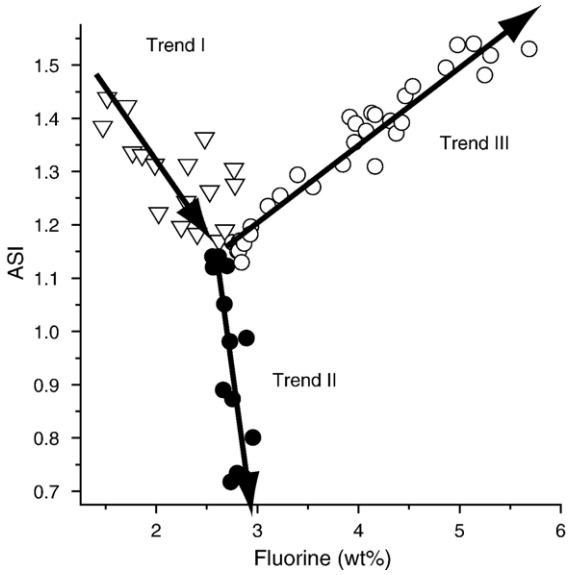

Fig. 4. Plot of ASI versus fluorine concentration of melt inclusions in quartz of the topaz–albite granite from Zinnwald showing three unique trends of melt evolution.

and an ASI ~ 1.15). These melts are homogeneous and represent the primary magmatic evolution, characterized by fractional crystallization and continuous enrichment of H_2O, F, Cl, and B up to saturation. At this saturation point, the primary homogeneous melt splits into two different fractions with contrasting properties. Trend II shows a strong negative correlation between ASI and F and represents the increasingly peralkaline trend (H_2O-rich type-B melt containing 20 to 55 wt.% H_2O). In trend III (the peraluminous trend, H_2O-poor type-A melt with 20–30 down to 5 wt.% H_2O), the ASI and F are strongly positively correlated as manifested in the initial trend I. The ratio ASI_A/ASI_B increases from 1 at the critical point to about 2.8 at 550 °C.

3.2. Melt compositions

From the extensive electron microprobe and Raman data acquired to date (e.g., Webster et al., 2004; Thomas et al., 2005) we have developed a simplified SiO_2–Al_2O_3–Na_2O–K_2O–F–H_2O model system, which can be used for the interpretation of the late-stage evolution of a complex granitic system (Fig. 5). Starting from the critical point (CP), a strong fractionation of SiO_2, Al_2O_3, alkalis, F, and H_2O is observed. Other elements (Zr, Hf, REE, etc.) behave accordingly as discussed briefly in the following section.

The different melt fractions are generally very volatile-rich and can, therefore, exsolve vapour phases with a strongly contrasting acidic or basic character,

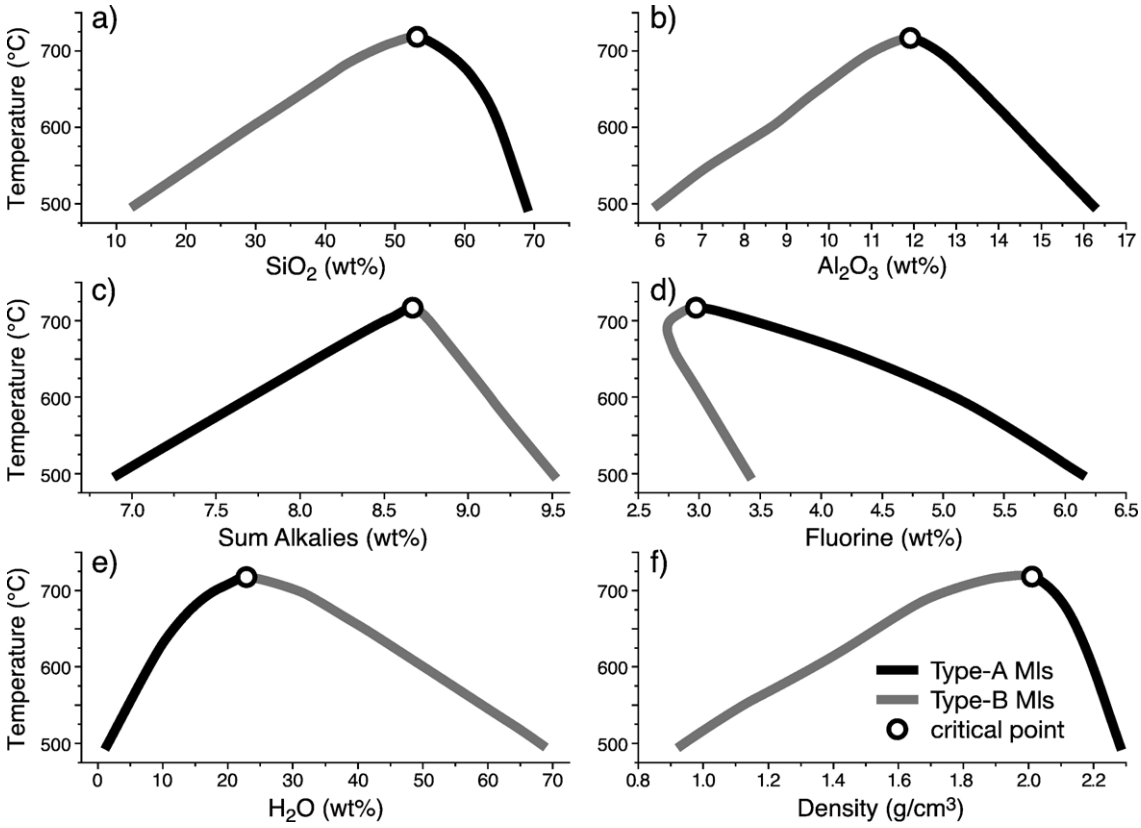

Fig. 5. SiO_2–Al_2O_3–Na_2O–K_2O–F–H_2O model system representing the topaz–albite granite system from Zinnwald (data from Thomas et al., 2005). Plots of temperature vs. (a) wt.% SiO_2, (b) wt.% Al_2O_3, (c) wt.% total alkalies (Na, K, Rb, Cs), (d) wt.% F, (e) wt.% H_2O, and (f) density of melt fractions. Starting from the critical point (CP), we observe a strong fractionation of SiO_2, Al_2O_3, alkalies, F, and H_2O. In figure (f), we have used the program of Herzberg (1987) to calculate a density–temperature diagram for this model system, showing that, starting at the CP, the density of the type-B melts decreases strongly with temperature.

depending on pressure and temperature. Such contrasting fluids have been found in single growth zones in quartz from several Sn–W deposits (Thomas et al., 2000, 2003, 2005). Because of their low viscosity and favourable wetting properties (Audétat and Keppler, 2004), the extremely H_2O- and F-rich peralkaline melts or silicate-rich solutions are excellent extraction media for incompatible elements. Isolated in the quartz hosts, crystalline remnants of the peralkaline evolution, such as nepheline, rubidian leucite, cryolite, cryolithionite, and elpasolite occur. Also common are clusters (>50–100 μm in diameter) of cryolite, topaz, fluorite, and albite crystals in quartz, reflecting strong enrichment in F (e.g., Dolejš and Baker, 2004). London (2005) ascribed the formation of cryolite inclusions in quartz to the presence of a sodic boundary layer sufficiently enriched in F. However, these clusters are too large and abundant to be explained by the boundary-layer effect. Very low-density melts are able to rapidly move upwards from their site of formation, in which case they are not necessarily in equilibrium with the adjacent mineral assemblages. Such fast-moving melts can feed growing crystals to large sizes (Beus, 1983).

By extraction of incompatible elements such as Nb, Ta, W, and Sn from the cumulate residuum (e.g., the main granite body), the peralkaline melt fractions may form rare-metal deposits of the Zr–Hf–Nb–Ta–REE type. The high concentration of F is responsible for complexing the REEs and other high field strength elements, indicated for example by the frequently occurring Y-REE fluorite in the region. In Zinnwald, this mineralization type occurs preferentially as disseminations in the intergranular space of the granite. Synchrotron XRF measurements of single type-B MIs in quartz from Zinnwald showed that such peralkaline melts may actually contain high concentrations of ore-forming elements (Thomas et al., 2005). The following average concentrations were determined (in ppm on an H_2O-free basis): Sn 850, Nb 1130, Mo 485, Rb 8830, Cs 4830, and some tens of ppm of Ta and W. Moreover,

wolframoixiolite occurs as a daughter mineral in this inclusion type, as it does in the type-B MIs from Ehrenfriedersdorf.

The processes and melt varieties discussed here do not represent vanishingly small quantities of melt that have little geological significance after formation. Rather, estimates of the amount of such residual melts in Zinnwald imply that these peralkaline melt fractions were present in volumes sufficiently large (1.3–6.6 km^3) to account for a great part of the ore mineralization (Thomas et al., 2005).

The Zinnwald example demonstrates two possibilities: (i) "in situ" enrichment of the incompatibles within the intergranular space of the crystallizing body, forming a disseminated ore mineralization, or (ii) extraction and transport away from the source and formation of ore concentrations in separate bodies (veins, pockets, etc.).

The separation of the melt from the crystal phases is crucial for this process and increases the alkali concentrations in the mobile part. This evolution also results in an increase of the H_2O concentration in the melt, since the addition of Na_2O up to peralkaline levels almost doubles the low-pressure (500 bar) solubility of H_2O in the melt (Dingwell et al., 1997). If the separation of the peralkaline melt fraction from the matrix is not complete, this evolution is a kind of autometasomatism.

3.3. Compositions of accessory minerals from contrasting melt fractions

Quartz phenocrysts locally contain crystals of rubidian leucite of the composition $(K_{0.64}Rb_{0.22}Na_{0.13}Cs_{0.01})_{1.00}(Al_{0.96}Fe_{0.03})_{0.99}Si_2O_6$. Leucite, as a feldspathoid, is found only in alkaline, silica-deficient rocks and is, therefore, a strong marker of (per)alkaline melt compositions. In addition to leucite, the following minerals were identified by Raman spectroscopy (see Thomas et al., 2005): cryolite (Na_3AlF_6), elpasolite (K_2NaAlF_6), cryolithionite ($Li_3Na_3Al_2F_{12}$), topaz, REE-rich fluorite, Nb-rich cassiterite (up to 4.0 wt.% Nb_2O_5 according to EMPA), rutile, Nb-tantalates, wolframoixiolite, Hf-rich zircon, monazite and xenotime (see Tables 2a and 2b). These accessory minerals are usually very small, mostly <50 μm in diameter, compositionally heterogeneous, corroded, fractured, embayed and contain abundant holes. Many of these accessory crystals are also complexly zoned. These features are consistent with rapidly changing chemical conditions during crystal growth and renewed dissolution. In contrast, the centimeter-size cassiterite crystals from peraluminous environments are pure, containing only 0.09 wt.% Nb_2O_5.

Because type-B MIs, which represent extremely H_2O- and F-rich silicate melts with more than 20 wt.% H_2O (see Thomas et al., 2000, 2003), contain Y-REE fluorides, cryolite and wolframoixiolite, we suggest that most of these accessory minerals crystallized from the peralkaline melt fraction.

4. Other examples of the formation of strongly peralkaline melt fractions

Since most evidence of preexisting peralkalinity is removed by the high reactivity of such melts or liquids, it is difficult, but important to find evidence of such an evolution. Very high alkali-element concentrations (20–40 wt.%) in volatile-rich melts were measured in inclusions in the Precambrian pegmatites from Bornholm (Thomas, 2003). Nahcolite- and zabuyelite (Li_2CO_3)-rich salt-melt inclusions in pegmatite feldspar and quartz, together with type-B MIs, were observed, whereas type-A MIs are subordinate. Veksler (2004) has shown that melt–melt immiscibility is favoured in peralkaline melts containing high concentrations of H_2O, F, Cl, B, and CO_3^{2-}, and we suggest that the dominance of alkalies in the Bornholm MIs implies that the chemical evolution via melt–melt immiscibility has progressed towards very high alkalinity. The occurrence of high concentrations of alkali carbonates and bicarbonates is an indirect indication of peralkaline melt and fluid fractions (see Thomas et al., 2006a), because $Na_2Si_2O_5$ (sodium disilicate) is unstable in the presence of CO_2 at room temperature (Mustart, 1972).

The study of pegmatites from Malkhan (Transbaikalia) (Thomas et al., 2002; Thomas and Badanina, 2005) shows that magma evolution progressed towards extremely volatile-rich melt fractions, formed during cooling along a solvus boundary in an X_{H2O}–T pseudobinary melt system (see Table 4).

Studies of peralkaline granites from the Brandberg-Amis Complex (Schmitt et al., 2002) demonstrate formation of melts with strongly different composition by melt–melt immiscibility (R. Thomas, unpublished results). Fig. 6 shows a MI in quartz after re-homogenization at 700 °C and 1 kbar. Table 5 lists the composition of the two different MIs, as well as the bulk composition of the granite. Since this inclusion randomly trapped a globule of type-B melt within a volume of type-A melt, this photomicrograph indicates the initial scale of the exsolution of immiscible phases. Subsequent accumulation and ponding may have occurred in the pegmatite, but the initial exsolution

Table 4
Average compositions (wt.%) of type-A and type-B melt inclusions in quartz from the Malkhan pegmatite field (Central Transbaikal region, Russia), re-homogenized at 700 °C and 1 kbar—re-calculated to a sum of 100/water-free basis

	Type-A MIs	Type-B MIs
SiO_2	72.00	66.30
TiO_2	0.03	0.01
B_2O_3	2.90±0.95	7.02±0.80
Al_2O_3	12.62	10.44
MgO	d.l.	d.l.
CaO	0.11	0.05
Li_2O (estimated)	1.50	1.29
Na_2O	2.95	4.34
K_2O	3.05	4.00
Rb_2O	0.21	0.14
Cs_2O	2.95	3.49
F	1.61	2.89
Cl	d.l.	0.01
P_2O_5	0.04	0.02
H_2O	11.7±2.5	25±6.0
ASI	1.32	0.81
ASI (+Li)	0.86	0.60
n	18	30

d.l.—below detection limit.
n—number of determined MIs.

appears to have begun on a very small scale (i.e., globules of only a few micrometers in diameter).

Preston et al. (2003) showed experimentally that a pseudobinary solvus is generated in silica-undersaturated alkaline magmas at 850 °C and 1 kbar. This solvus also generates a strong chemical polarization between the silicate melt and the coexisting fluids that were

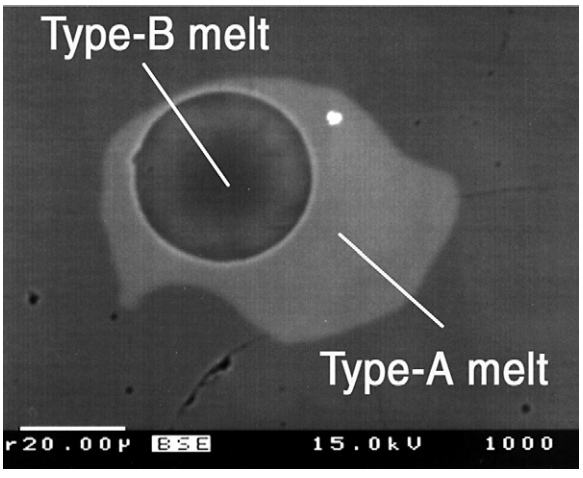

Fig. 6. A melt inclusion in quartz from the Amis Complex, Namibia, after re-homogenization at 700 °C and 1 kbar. The inclusion consists of a globule of volatile-rich silicate glass representing type-B melt embedded in a volatile-poorer type-A melt. The white spot in the type-A melt is a small zircon crystal.

Table 5
Mean compositions (wt.%±1σ) of the bulk rock (granite) and type-A and type-B melts from the Amis Complex (Namibia)—re-calculated to a sum of 100/water-free basis

	Granites	Type-A MIs	Type-B MIs
Nb_2O_5	<0.32	n.d.	0.58±0.16
Ta_2O_5	<0.01	n.d.	0.09±0.04
SiO_2	73.1±1.2	69.5±1.2	66.0±1.0
TiO_2	0.25±0.10	0.48±0.16	0.63±0.14
ZrO_2	0.15±0.10	0.50±0.28	1.09±0.07
SnO_2	n.d.	0.04	0.08±0.02
Al_2O_3	10.1±0.7	12.9±1.00	9.02±0.12
B_2O_3	n.d.	n.d.	0.79
Y_2O_3	0.10	0.15±0.08	0.23±0.08
Ce_2O_3	0.02	0.09±0.03	0.14+0.05
FeO	4.89±1.00	2.76±0.66	3.61±0.34
MnO	0.07±0.02	0.10±0.02	0.16±0.03
MgO	0.03	0.02	<0.05
CaO	0.09	0.24±0.10	<0.05
Na_2O	5.17±0.85	4.37±1.16	5.18±0.23
K_2O	4.51±0.43	5.92±0.79	5.22±0.28
Rb_2O	0.08±0.04	0.36±0.07	0.36±0.03
Cs_2O	0.001	n.d.	0.05±0.02
F	0.50±0.05	2.39±0.30	4.54±0.50
Cl	n.d.	0.13±0.03	0.17±0.08
P_2O_5	0.10±0.01	<0.05	0.05
CO_3^{2-}	n.d.	n.d.	1.83±0.20
Sum (dry)	99.49	100.04	99.92
H_2O	n.d.	15.5±0.8	34.7±2.7
ASI	0.74±0.09	0.91±0.15	0.62±0.02
n	8	15	30

n—analysed MIs or samples.
n.d.—not detected.

highly enriched in dissolved solids (in the range of 40–50 wt.% $SiO_2+Al_2O_3+Na_2O$). The ASI melt/fluid ratio is approximately 1.00 to 0.41. Given large enough quantities, such a fluid could metasomatize a typical granodiorite to a nepheline syenite by fluid/rock interaction. The discovery of nepheline in the pegmatite quartz from Ehrenfriedersdorf is striking evidence that such processes actually take place in nature.

5. Discussion

In order to investigate how melt–melt immiscibility may occur at a molecular level, we have calculated and constructed a density–temperature diagram (see Fig. 5f), using the methods of Herzberg (1987) and compositional data from Zinnwald. The two immiscible conjugate melts are characterized by strong differences in melt structure as visualized by the fast Brownian movement of particles in the melt. The type-A melts are relatively highly polymerized, whereas the type-B melts have a strongly depolymerized structure. According to Raman spectroscopy as well as HDAC experiments, the

behaviour of homogeneous melts formed near the critical point of the solvus is similar to a brine (see Fig. 7). Furthermore, the HDAC experiments show clearly that a silicate melt is completely soluble in a water-rich solution, demonstrating that there is a continuous transition between the two extremes (see Roedder, 1984a, p. 397).

Fluorine, together with H_2O, strongly reduces the viscosity of silicate melts due to depolymerization (Dingwell, 1987; Giordano et al., 2004). The complex interplay of the volatiles H_2O, F, and Cl, the semi-volatiles B and P, and fluxing components such as Be, B, Li, Rb, and Cs, along with Si, Al, Na and K, in a strongly depolymerized melt is responsible for the peculiar immiscibility behaviour, here at low temperature (~ 700 °C) and pressures of about 1 kbar (see Thomas et al., 2000).

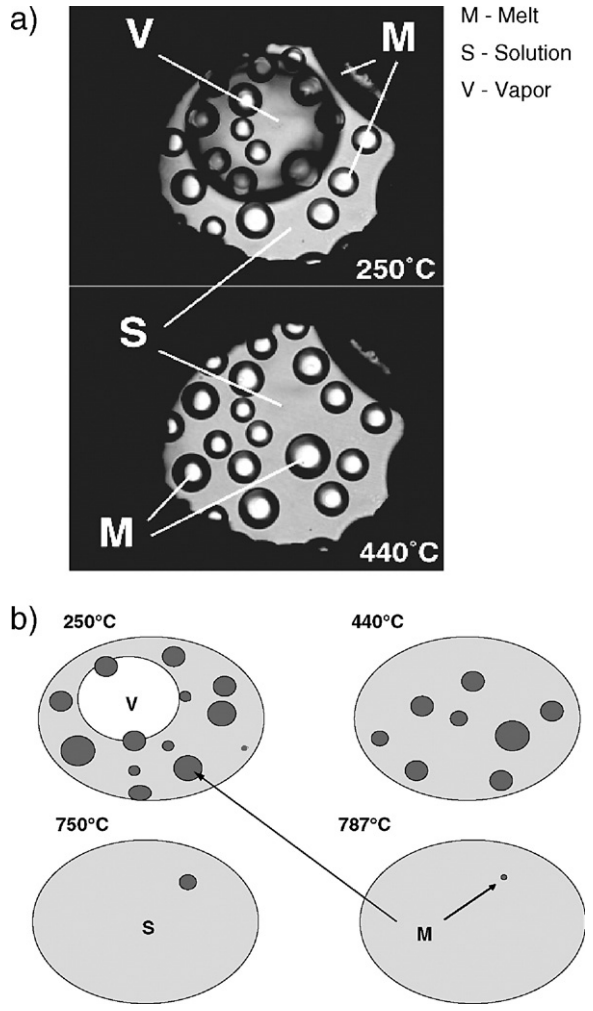

Fig. 7. (a) Photomicrographs of typical HDAC experiments in the Al_2O_3–Na_2O–K_2O–H_2O system showing droplets of silicate melt (M) in an aqueous fluid (S) and a vapor bubble (V) at 250 °C. The lower photo shows droplets of silicate melt (M) in an aqueous fluid (S) at 440 °C. (b) shows schematically the homogenization behavior of a melt inclusion with similar phase composition. Total homogenization in the solution occurs at 787 °C according to the scheme (melt + solution→solution).

Because of the strong viscosity and density contrasts, physical separation of both melts should be efficient. Melts of such low viscosity can form an interconnected network, sequester potential ore metals, and can move over large distances from the source, allowing ore components to accumulate at the top of magma cupolas prior the completion of magmatic crystallization. The low viscosity of the volatile-rich melt fraction is demonstrated by the high mobility of small bubbles, small daughter crystals or tiny opaque phases observed under the microscope during the MI homogenization measurements or HDAC experiments (e.g., Fürth, 1930; Thomas, 1979). Based on this mobility, Fürth (1930) presented a simple method of determining viscosity using Einstein's essential contribution on Brownian motion from 1905 (see Einstein, 1956). The fast Brownian movement in an inclusion, or in the hydrothermal diamond cell (HDAC), is a very good means of visualizing this important melt property (see Thomas, 1979; Veksler et al., 2002). The MI inventory in double-terminated quartz crystals ("Schwimmer") found in quartz veins in gneiss some 10's of meters outside the granite body supports the idea that the volatile-rich, pegmatite-forming melt is highly mobile. These quartz crystals contain a core (1/3 of the volume) containing both type-A and type-B MIs surrounded by colourless quartz of hydrothermal origin. These crystals provide compelling evidence for the migration of volatile-rich melt fractions over at least tens of meters.

6. Summary

If crystal fractionation-driven enrichment of F and H_2O in granite-forming melts approaches values of about 2.6 wt.% F and 20 to 25 wt.% H_2O, the primary, homogeneous residual silicate melt is no longer stable at low pressures (about 1 kbar) and separates into two conjugate melt fractions by liquid immiscibility (Fig. 8). One fraction is peraluminous, while the other is peralkaline. These melt fractions have strongly contrasting chemical and physical properties and will tend to separate readily from each other. Many incompatible elements (for example Hf) will be extracted from the crystallizing mass and removed into the mobile phase by chromatographic effects. Once melt–melt immiscibility has occurred, each melt may respond independently to the changing conditions, and a second- or third-order

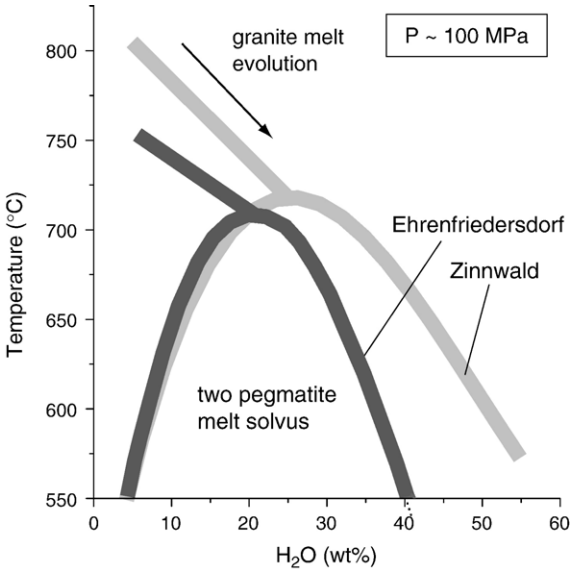

Fig. 8. Pseudobinary solvus (H_2O versus temperature) at volatile saturation caused by fractional crystallization of the Zinnwald and Ehrenfriedersdorf magmas (see text for discussion).

melt separation by immiscibility is possible. Such processes may result in further enrichment of certain incompatible elements such as Sc, Zr, Hf, Nb, Ta, or Sn as observed in some pegmatites.

The separation of a mobile phase from the cumulate residuum causes an increase of the peraluminosity of the residuum and of the alkalinity of the mobile phase. This mobile phase can react as a metasomatic agent (see Beus, 1983; Preston et al., 2003) or may form separate pegmatite bodies with different bulk composition. Unfortunately, an intense greisenization stage can remove all evidence of the action of a former peralkaline fluid or melt. Therefore, the pegmatites and MIs are the only remnants of this melt separation in granitic systems.

If the separated peralkaline melt fraction intrudes into the dominantly peraluminous host rocks, with which it is in strong disequilibrium, it will react until equilibrium is attained. Therefore, the peralkaline character is often preserved only in the isolated inclusions (mineral or melt). In high level intrusions, a large quantity of alkalis will leave the system due to extensive hydrothermal activity and produce a rock higher in peraluminosity index than the original magma.

Acknowledgements

We thank the Geoscientific Collections at the Faculty of Earth Sciences, Geotechnics and Mining of the TU Bergakademie Freiberg for crucial samples from the tin-tungsten deposit Ehrenfriedersdorf, as well as E. Badanina for samples from the Malkhan pegmatite field, Transbaikalia. We thank Mrs. O. Appelt for help with EMP analysis, G. Berger for preparation of numerous samples, and Mrs. H. Steigert for performing several high-pressure re-homogenization experiments. We wish to express our appreciation to C. Schmidt, R. Schulz and I. Veksler for the preparation and performing of some of the crucial HDAC experiments. The work has benefited from stimulating discussions with I. Veksler, E. Badanina, S. Smirnov, D. Kamenetsky, and A. Anderson.

The study was supported by the Deutsche Forschungsgemeinschaft (DFG) through the grant Th 489 to R. Thomas and W. Heinrich, and was in part conducted within the framework of the DFG Priority Program SPP 1055 “Bildung, Transport und Differenzierung von Silikatschmelzen”. The constructive comments of editor G. Markl, and the reviews of R. Seltmann and an anonymous referee greatly improved this paper.

References

Audétat, A., Keppler, H., 2004. Viscosity of fluids in subduction zones. Science 303, 513–516.

Beus, A., 1983. On the possible mechanism of formation of euhedral crystals in metasomatic processes. Bull. Mineral. 106, 411–415.

Bühn, B., Wall, F., Le Bas, M.J., 2001. Rare-earth element systematics of carbonatitic fluorapatites, and their significance for carbonatite magma evolution. Contrib. Mineral. Petrol. 141, 572–591.

Chakhmouradian, A.R., Mitchell, R.H., 2002. The mineralogy of Ba- and Zr-rich alkaline pegmatites from Gordon Butte, Crazy Mountains (Montana, USA): comparisons between potassic and sodic agpaitic pegmatites. Contrib. Mineral. Petrol. 143, 93–114.

Dingwell, D.B., 1987. Melt viscosities in the system $NaAlSi_3O_8$–H_2O–F_2O_{-1}. Magmatic Processes: Physicochemical Principles. Spec. Publ.-Geochem. Soc., vol. 1, pp. 423–431.

Dingwell, D.B., Holtz, F., Behrens, H., 1997. The solubility of H_2O in peralkaline and peraluminous granitic melts. Am. Mineral. 82, 434–437.

Dolejš, D., Baker, D.R., 2004. Thermodynamic analysis of the system Na_2O–K_2O–CaO–Al_2O_3–SiO_2–H_2O–F_2O_{-1}: stability of fluorine-bearing minerals in felsic igneous suites. Contrib. Mineral. Petrol. 146, 762–778.

Dudkin, O.B., Kosyreva, L.V., Pomeranceva, N.G., 1964. Mineralogy of the apatite deposits in the Khibina tundra. Nauka SSSR, Moskva and Leningrad. 236 pp. (in Russ.).

Einstein, A., 1956. Investigations on the theory of Brownian movement. Edited and annotated by R. Fürth. Unabridged, Unaltered Republication of the 1st (1926) English edition. Dover Publication, INC. 122 pp.

Fürth, R., 1930. Über die Messung der Viskosität sehr kleiner Flüssigkeitsmengen mit Hilfe der Brownschen Bewegung. Z. Phys. 60, 313–331.

Giordano, D., Romano, C., Dingwell, D.B., Poe, B., Behrens, H., 2004. The combined effects of water and fluorine on the viscosity of silicic magmas. Geochim. Cosmochim. Acta 68, 5159–5168.

Herzberg, C.T., 1987. Magma density at high pressure: Part 1. The effect of composition on the elastic properties of silicate liquids. In: Mysen, B. (Ed.), Magmatic Processes: Physicochemical Principles, Special Publication, vol. 1. The Geochemical Society, pp. 25–46.

Keppler, H., 1993. Influence of fluorine on the enrichment of high field strength trace elements in granitic rocks. Contrib. Mineral. Petrol. 114, 479–488.

London, D., 2005. Granite pegmatites: an assessment of current concepts and directions for the future. Lithos 80, 281–303.

Lowenstern, J.B., 2003. Melt inclusions come of age: volatiles, volcanoes, and Sorby's legacy. In: de Vivo, B., Bodnar, R.J. (Eds.), Melt Inclusions in Volcanic Systems—Methods, Applications and Problems. Elsevier Science B.V., pp. 1–21.

Mustart, D.A., 1972. Phase relations in the peralkaline portion of the system Na_2O–Al_2O_3–SiO_2–H_2O. PhD thesis, Stanford University, USA. 187 pp.

Mysen, B.O., Cody, G.D., Smith, A., 2004. Solubility mechanisms of fluorine in peralkaline and meta-aluminous silicate glasses and in melts to magmatic temperatures. Geochim. Cosmochim. Acta 68, 2745–2769.

Niggli, P., 1937. Das Magma und seine Produkte: I. Teil: Physikalisch-chemische Grundlagen. Akademische Verlagsgesellschaft M.B.H. Leipzig. 379 pp.

Oelsner, O., 1952. Die pegmatitisch-pneumatolytischen Lagerstätten des Erzgebirges mit Ausnahme der Kontaktlagerstätten. Freiberger Forschungshefte C4. 80 pp.

Preston, R.F., Stevens, G., McCarthy, T.S., 2003. Fluid compositions in equilibrium with silica-undersaturated magmas in the system Na_2O–Al_2O_3–SiO_2–H_2O: clues to the composition of fenitizing fluids. Contrib. Mineral. Petrol. 144, 559–569.

Rickers, K., Thomas, R., Heinrich, W., 2006. The behavior of trace elements during the chemical evolution of the H2O-, B-, and F-rich granite–pegmatite-hydrothermal system at Ehrenfriedersdorf, Germany: a SXRF study of melt and fluid inclusions. Miner. Depos. doi:10.1007/s00126-006-0057-7.

Roedder, E., 1984. Fluid inclusions. Rev. Miner. 12. 644 pp.

Romer, R., Thomas, R., 2005a. U–Pb dating of primary tin mineralization at Ehrenfriedersdorf using micro-inclusions. Eur. J. Mineral. Suppl. 17, 111.

Romer, R.L., Thomas, R., 2005b. U–Pb dating of micro-inclusions: the age of the Ehrenfriedersdorf tin deposit (Erzgebirge, Germany). In: Jingwen, Mao, Bierlein, F.P. (Eds.), Mineral Deposits Research: Meeting the Global Challenge. Proceedings 8th Biennial SGA Meeting Beijing, China, 18–21 August 2005, pp. 817–820.

Schmitt, A.K., Trumbull, R.B., Dulski, P., Emmermann, R., 2002. Zr–Nb–REE mineralization in peralkaline granites from the Amis Complex, Brandberg (Namibia): evidence for magmatic pre-enrichment from melt inclusions. Econ. Geol. 97, 399–413.

Schmidt, C., Thomas, R., Heinrich, W., 2005. Boron speciation in aqueous fluids at 22 to 600 °C and 0.1 MPa to 2 GPa. Geochim. Cosmochim. Acta 69, 275–281.

Thomas, R., 1979. Investigation of inclusions for the thermodynamic and physico-chemical characterization of ore-forming solutions and processes in the magmatic and postmagmatic range (in German). Unpublished Dissertation A, Bergakademie Freiberg, 245 pp.+83 pp. Supplement.

Thomas, R., 2000. Determination of water contents of granite melt inclusions by confocal laser Raman microprobe spectroscopy. Am. Mineral. 85, 868–872.

Thomas, R., 2003. Melt and fluid inclusions in evolved and simple granite pegmatites. Acta Mineral.-Petrogr., Abstr. Ser. 2, 211–212 (Szeged).

Thomas, R., Badanina, E.V., 2005. Evolution of silicate melts during formation of the granite–pegmatite system of the Malkhany pegmatite field, Russia, ECROFI 2005, CD.

Thomas, R., Tischendorf, G., 1987. Evolution of Variscan magmatic-metallogenetic processes in the Erzgebirge according to thermometric investigations. Z. Geol. Wiss. 15, 25–42.

Thomas, R., Webster, J.D., Heinrich, W., 2000. Melt inclusions in pegmatite quartz: complete miscibility between silicate melts and hydrous fluids at low pressure. Contrib. Mineral. Petrol. 139, 394–401.

Thomas, R., Badanina, E., Veksler, I., 2002. Extreme Boron Enrichment in Granitic Melt Revealed by Melt Inclusions from Malkhan Pegmatite, Russia, PACROFI VIII, July 21–26. Halifax, Nova Scotia, Canada, pp. 106–107.

Thomas, R., Förster, H.-J., Heinrich, W., 2003. The behaviour of boron in a peraluminous granite–pegmatite system and associated hydrothermal solutions: a melt and fluid inclusion study. Contrib. Mineral. Petrol. 144, 457–472.

Thomas, R., Förster, H.-J., Rickers, K., Webster, J.D., 2005. Formation of extremely F-rich hydrous melt fractions and hydrothermal fluids during differentiation of highly evolved tin-granite magmas: a melt/fluid-inclusion study. Contrib. Mineral. Petrol. 148, 582–601.

Thomas, R., Webster, J.D., Davidson, P., 2006a. Understanding pegmatite formation: the melt and fluid inclusion approach. GAC-MAC Short Course 36, 189–210.

Thomas, R., Kamenetsky, D., Davidson, P., 2006b. Laser Raman spectroscopic measurements of water in unexposed glass inclusions. Am. Mineral. 91, 467–470.

Veksler, I.V., 2004. Liquid immiscibility and its role at the magmatic-hydrothermal transition: a summary of experimental studies. Chem. Geol. 210, 7–31.

Veksler, I.V., Thomas, R., Schmidt, C., 2002. Experimental evidence of three coexisting immiscible fluids in synthetic granite pegmatite. Am. Mineral. 87, 775–779.

Vogel, W., 1977. Phase Separation in Glass. Glass'77, XIth International Congress on Glass, Prague, July 4–8, pp. 170–214.

Webster, J.D., Thomas, R., Rhede, D., Förster, H.-J., Seltmann, R., 1997. Melt inclusions in quartz from an evolved peraluminous pegmatite: geochemical evidence for strong tin enrichment in fluorine-rich and phosphorus-rich residual liquids. Geochim. Cosmochim. Acta 61, 2589–2604.

Webster, J., Thomas, R., Förster, H.-J., Seltmann, R., Tappen, Ch., 2004. Geochemical evolution of halogen-enriched granite magmas and mineralizing fluids of the Zinnwald tin-tungsten mining district, Erzgebirge, Germany. Miner. Depos. 39, 452–472.